Observation of Time-Reversal-Protected Single-Dirac-Cone Topological-Insulator States in Bi_2Te_3 and Sb_2Te_3

D. Hsieh,[1] Y. Xia,[1] D. Qian,[1] L. Wray,[1] F. Meier,[2,3] J. H. Dil,[2,3] J. Osterwalder,[3] L. Patthey,[2] A. V. Fedorov,[4] H. Lin,[5] A. Bansil,[5] D. Grauer,[6] Y. S. Hor,[6] R. J. Cava,[6] and M. Z. Hasan[1,*]

[1]*Joseph Henry Laboratories of Physics, Princeton University, Princeton, New Jersey 08544, USA*
[2]*Swiss Light Source, Paul Scherrer Institute, CH-5232, Villigen, Switzerland*
[3]*Physik-Institut, Universität Zürich-Irchel, 8057 Zürich, Switzerland*
[4]*Advanced Light Source, Lawrence Berkeley National Laboratory, Berkeley, California 94720, USA*
[5]*Department of Physics, Northeastern University, Boston, Massachusetts 02115, USA*
[6]*Department of Chemistry, Princeton University, Princeton, New Jersey 08544, USA*

(Received 18 June 2009; published 28 September 2009)

We show that the strongly spin-orbit coupled materials Bi_2Te_3 and Sb_2Te_3 and their derivatives belong to the Z_2 topological-insulator class. Using a combination of first-principles theoretical calculations and photoemission spectroscopy, we directly show that Bi_2Te_3 is a large spin-orbit-induced indirect bulk band gap ($\delta \sim 150$ meV) semiconductor whose surface is characterized by a single topological spin-Dirac cone. The electronic structure of self-doped Sb_2Te_3 exhibits similar Z_2 topological properties. We demonstrate that the dynamics of spin-Dirac fermions can be controlled through systematic Mn doping, making these materials classes potentially suitable for topological device applications.

DOI: 10.1103/PhysRevLett.103.146401 PACS numbers: 71.20.−b, 71.10.Pm, 73.20.At, 73.23.−b

Topological insulators are a new phase of quantum matter that host exotic Dirac electrons at their edges owing to a combination of relativistic and quantum entanglement effects [1]. They were recently proposed [2–4] and shortly afterwards discovered in the $Bi_{1-x}Sb_x$ [5,6] and Bi_2Se_3 [7,8] materials. In these systems, spin-orbit coupling (SOC) gives rise to electrically insulating states in the bulk and robust conducting states along the edges. In contrast to graphene, which has four Dirac cones (2 doubly degenerate cones at the K and K' points in momentum space) [9], the remarkable property of topological edge states is that their dispersion is characterized by an odd number of nondegenerate Dirac cones. Such odd Dirac-cone edge metals are predicted to exhibit a host of unconventional properties including a fractional (half-integer) quantum Hall effect [2,10] and immunity to Anderson localization due to spin-texture and pi Berry's phases on their surfaces [2,5–7,11]. The most exciting physics, however, may occur at the interface between a topological insulator and an ordinary ferromagnet or superconductor, where electromagnetic responses that defy Maxwell's equations [10,12,13] and excitations that obey non-Abelian statistics [14,15] have been predicted.

The surging number of interesting experimental proposals involving odd Dirac-cone surface metals [10,14–17] has ignited a search for the most elementary form of a topological insulator, namely, one with a large bulk band gap and a single surface Dirac cone. Although $Bi_{1-x}Sb_x$ has a room temperature direct band gap ($\delta > 30$ meV) [5], a small effective mass of its bulk electrons is known to cause the system to form conducting impurity bands even in high purity samples [18], which dominate over conduction through the surface states. More importantly, $Bi_{1-x}Sb_x$ has multiple surface states of both topological and nontopological origin [5], which makes isolating any transport signal from a single topological surface state particularly challenging. More recently, angle-resolved photoemission spectroscopy (ARPES) and theoretical [7,19] evidence suggest that Bi_2Se_3 is a large band gap (~300 meV) single-Dirac-cone topological insulator. In this Letter, we report a bulk and surface ARPES investigation of single crystals of Bi_2Te_3, $Bi_{2-x}Mn_xTe_3$, and Sb_2Te_3. Remarkably, we find that their electronic structures are in close agreement with our topological SOC calculations shown here, and a single Dirac cone is realized on their (111) surface. Although Sb_2Te_3 is found to have stable gapless bulk states, we show that the Fermi energy of Bi_2Te_3 is time dependent, which has also been observed with ARPES in hole-doped Bi_2Te_3 samples [20], and can be controlled via Mn doping. Using a synchrotron light source with a variable photon energy ($h\nu$), we show that the bulklike states of $Bi_{2-x}Mn_xTe_3$ ($x = 0$) are insulating with the valence band maximum lying around 150 meV below E_F, realizing a large band gap topological insulator with tunable surface dynamics that can be used for novel topological physics.

ARPES measurements were performed with 28–45 eV linearly polarized photons on beam line 12.0.1 at the Advanced Light Source in Lawrence Berkeley National Laboratory. The typical energy and momentum resolution was 15 meV and 1% of the surface Brillouin zone (BZ), respectively. Single crystals of $Bi_{2-x}Mn_xTe_3$ were grown by melting stoichiometric mixtures of elemental Bi (99.999%), Te (99.999%), and Mn (99.95%) at 800 °C overnight in a sealed vacuum quartz tube. The crystalline sample was cooled over a period of 2 days to 550 °C and maintained at the temperature for 5 days. The same proce-

dure was carried out with Sb (99.999%) and Te (99.999%) for Sb_2Te_3 crystals. Our calculations were performed with the linear augmented-plane-wave method in slab geometry using the WIEN2K package [21]. The generalized gradient approximation of Perdew, Burke, and Ernzerhof [22] was used to describe the exchange-correlation potential. Spin-orbit coupling was included as a second variational step using scalar-relativistic eigenfunctions as a basis. The surface was simulated by placing a slab of six quintuple layers in vacuum using optimized lattice parameters from Ref. [23]. A grid of $35 \times 35 \times 1$ points was used in the calculations, equivalent to 120 k points in the irreducible BZ and 2450 k points in the first BZ.

The most basic 3D topological insulator supports a single Dirac cone on its surface [Fig. 1(a)], with the Dirac node located at a momentum $\mathbf{k}_T$ in the surface BZ, where $\mathbf{k}_T$ satisfies $\mathbf{k}_T = -\mathbf{k}_T + \mathbf{G}$ and $\mathbf{G}$ is a surface reciprocal-lattice vector [2]. Our theoretical calculations on Bi_2Te_3 (111) show that it is a SOC-induced bulk band insulator and that a single surface Dirac cone that encloses $\mathbf{k}_T = \bar{\Gamma}$ appears only when SOC is included [Fig. 1(b)]. To determine whether single crystalline Bi_2Te_3 is a topological insulator as predicted, we first mapped its high energy valence bands using ARPES. Figures 1(c) and 2 show that the measured bulk band structure is well described by SOC calculations, suggesting that the electronic structure is topologically nontrivial. A more direct probe of the topological properties of Bi_2Te_3, however, is to image its

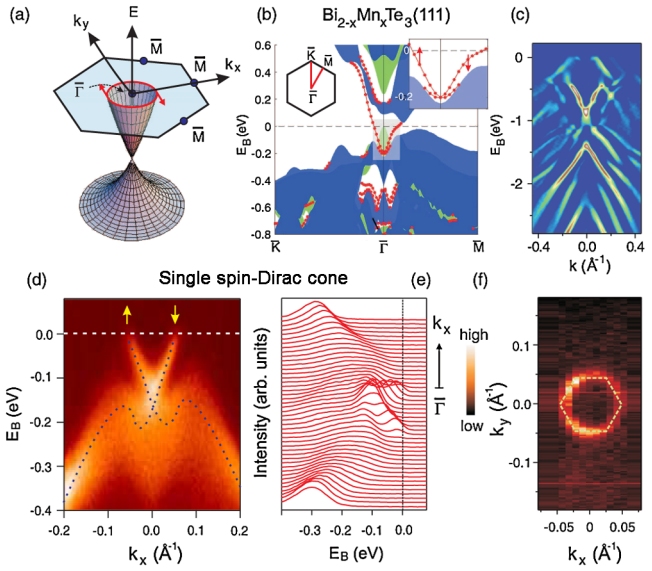

FIG. 1 (color online). A single massless topological spin-Dirac cone on the surface of $Bi_{2-x}Mn_xTe_3$: (a) Schematic of the (111) surface Brillouin zone with the four time-reversal-invariant momenta ($\bar{\Gamma}$, $3 \times \bar{M}$) marked by blue circles. A single Fermi surface enclosing $\bar{\Gamma}$ that arises from a Dirac cone is the signature of the most basic topological insulator. Red arrows denote the direction of spin [6] around the Fermi surface of a Dirac cone. (b) Calculated band structure along the $\bar{K} - \bar{\Gamma} - \bar{M}$ cut of the Bi_2Te_3(111) BZ. Bulk band projections are represented by the shaded areas. The band structure results with SOC are presented in blue and that without SOC in green. The magnitude of the bulk indirect gap is typically underestimated by *ab initio* calculations. No pure surface band is observed within the bulk band gap without SOC (black lines). One pure gapless surface band crossing E_F is observed when SOC is included (red lines). The inset shows an enlargement of the low energy region (shaded box) near $\bar{\Gamma}$. (c) ARPES second derivative image of the bulk valence bands of Bi_2Te_3 along $\bar{\Gamma} - \bar{M}$. (d) ARPES intensity map of the gapless surface state bands imaged 1 h after cleavage. The blue dotted lines are guides to the eye. The spin directions are marked based on calculations. (e) Energy distribution curves of the data shown in (d). (f) Constant energy ARPES intensity map collected at E_F using $h\nu = 35$ eV. Yellow dotted lines are guides to the eye.

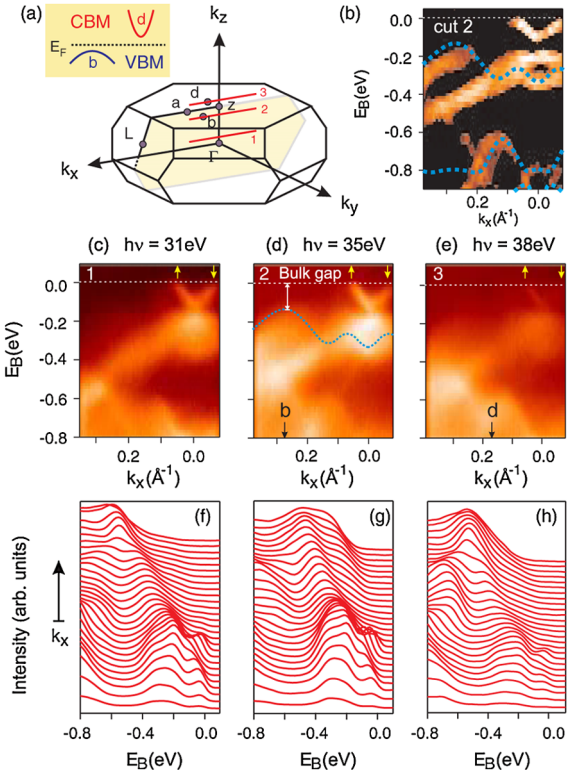

FIG. 2 (color online). Observation of insulating bulklike states in stoichiometric Bi_2Te_3 supporting a six-peak electronic structure: (a) bulk rhombohedral Brillouin zone of Bi_2Te_3. According to local-density approximation band structure calculations [24,25], six valence band maxima are located at the **b** points that are related to one another by 60° rotations about $\hat{z}$. The red lines show the momentum space trajectories of the ARPES scans taken using $h\nu = 31$, 35, and 38 eV. The inset shows a schematic of the indirect bulk band gap. (b) Calculated valence band structure along cut 2 superimposed on the second derivative image of a corresponding ARPES cut. The calculated band energies have been shifted downwards to match the data. (c)–(e) show ARPES intensity maps along the $h\nu = 31$, 35, and 38 eV trajectories, respectively, obtained 1 h after sample cleavage. The in-plane momentum components of the **b** and **d** points are marked by black arrows, and the energy of the valence band maximum relative to E_F (δ) is marked by a double-headed arrow. Yellow arrows denote the direction of the spin of Dirac-cone surface states. (f)–(h) show the energy distribution curves corresponding to images (c)–(e), respectively.

surface states. Figures 1(d) and 1(e) show that the surface states are metallic and are characterized by a single-Dirac-cone crossing E_F, in agreement with theory [Fig. 1(b)]. Moreover, the density of states at E_F is distributed about a single ring enclosing $\bar{\Gamma}$ [Fig. 1(f)], in accordance with Bi_2Te_3 being a topological insulator.

Our theoretical calculations show that stoichiometric Bi_2Te_3 is a bulk indirect gap insulator [Fig. 1(b)]. The bulk valence band maximum (VBM) in Bi_2Te_3 lies at the **b** point in the ΓZL plane of the three-dimensional bulk BZ [Fig. 2(b)], giving rise to a VBM in each of the six such mirror planes in agreement with previous proposals [24,25]. The VBM exhibits an indirect gap with the conduction band minimum (CBM) above E_F, which is located at the **d** point in the ΓZL plane. In order to establish whether Bi_2Te_3 is a bulk insulator as predicted, we performed a series of ARPES scans along the cuts shown by red lines in Fig. 2(a) (displaced along k_z by varying $h\nu$) that traverse the locations of the VBM and CBM in the bulk BZ. All $h\nu$-dependent scans were taken more than an hour after cleavage to allow the band structure to stabilize (see Fig. 3). Figures 2(c)–2(h) show a series of ARPES band dispersions along momentum cuts in the $k_x - k_z$ plane taken using $h\nu = 31$, 35, and 38 eV, respectively. The Dirac cone near E_F shows no dispersion with $h\nu$, supporting its surface state origin. In contrast, a strongly $h\nu$ dispersive holelike band is observed near $k_x = 0.27$ Å^{-1}, whose maximum rises to an energy δ closest to E_F ($\delta = -150 \pm 50$ meV) when $h\nu = 35$ eV [Fig. 2(d)]. Using the free electron final state approximation, the VBM is located at $(0.27, 0, 0.27)$ Å^{-1}, in agreement with calculations. ARPES scans taken in the vicinity of the **d** point $(0.17, 0, 0.37)$ Å^{-1}, which is traversed directly when $h\nu = 38$ eV, do not measure any signal from the CBM, showing that E_F lies in the bulk band gap. This is consistent with the size of the indirect band gap (>150 meV) measured using tunneling [26] and optical techniques [27]. We note that because ARPES is sensitive only to the topmost quintuple layer [Fig. 3(a)] at our sampled photon energies [28], the measured energy of the bulk band edge δ may differ from the true bulk value due to band bending effects that are commonly observed in semiconductors.

In order to investigate the effects of semiconductor band bending on the surface Dirac cone on Bi_2Te_3, we performed time-dependent ARPES experiments. Our results show that the binding energy of the Bi_2Te_3 surface Dirac node exhibits a pronounced time dependence, increasing from $E_B \sim -100$ meV 8 minutes after cleavage to $E_B \sim -130$ meV at 40 minutes [Figs. 3(c)–3(e)], in agreement with a previous report [20]. Such behavior has been attributed to a downward band bending near the surface [Fig. 3(b)] that is caused by the breaking of interquintuple layer van der Waals Te(1)—Te(1) bonds [Fig. 3(a)], which creates a net electric field near the surface upon crystal termination [25,26]. Unlike previous calculations [19], our calculated position of the Dirac node lies in the bulk band gap [Fig. 1(b)], which corroborates our experimental finding that the intensity is strongest near the Dirac node and drastically weakens away from $\bar{\Gamma}$ as the surface band merges with the bulk bands and become short-lived [5,6,28]. The slow dynamics of the band bending process suggests that charge accumulation at the surface is coupled to a much slower surface lattice relaxation [20]. The system is likely to be significantly delayed in achieving equilibrium by local lattice or charge density fluctuations such as may arise from site defects, which are prominent in such materials [8,26]. By systematically increasing the defect concentration through Mn for Bi substitution, we demonstrate here that band bending can be slowed by up to tenfold [Figs. 3(f)–3(h)], allowing a wider range of the intrinsic relaxation time scale to be accessed. ARPES valence band spectra [Fig. 3(i)] of $Bi_{1.95}Mn_{0.05}Te_3$ taken over a 15 h period show that the positions of the valence band edges shift downward by a total energy of around 100 meV, which we take as a measure of the total magnitude of band bending Δ.

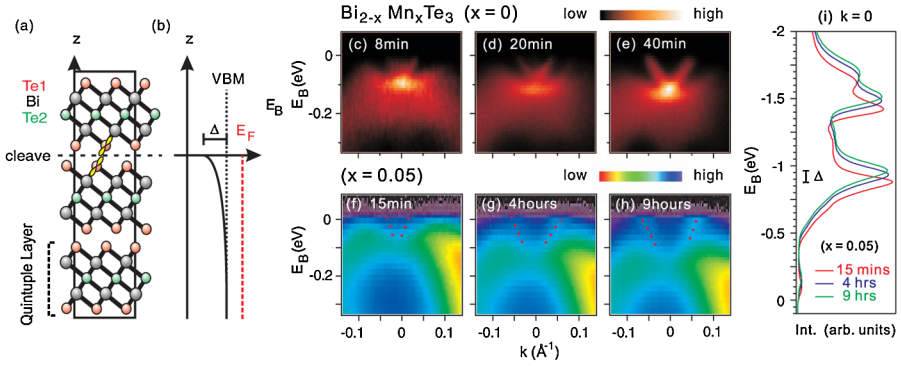

FIG. 3 (color online). Slow dynamics of the surface Dirac-cone dispersion in $Bi_{2-x}Mn_xTe_3$: (a) the crystal structure of Bi_2Te_3 viewed parallel to the quintuple layers. The Te(1) $5p$ orbitals that form the interquintuple layer van der Waals bonds are shown in yellow. (b) Schematic of the band bending of the bulk VBM near the cleaved surface. (c) ARPES spectra of Bi_2Te_3 along the $\bar{\Gamma}$-$\bar{M}$ direction taken with $h\nu = 30$ eV (c) 8, (d) 20, and (e) 40 min after cleavage in UHV. Analogous ARPES spectra for $Bi_{1.95}Mn_{0.05}Te_3$ (f) 15 min, (g) 4 h, and (h) 9 h after cleavage, showing a slower relaxation rate. Red lines are guides to the eye. (i) The energy distribution curves of $Bi_{1.95}Mn_{0.05}Te_3$ at $\bar{\Gamma}$ at various times after cleavage.

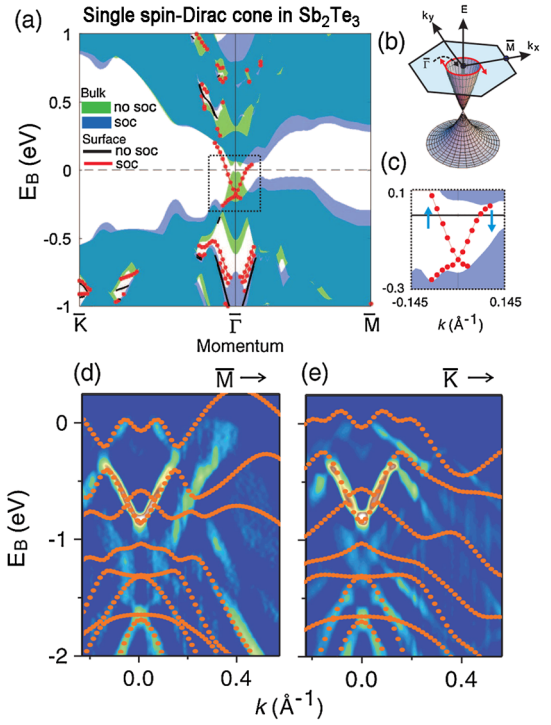

FIG. 4 (color online). Evidence for a topologically nontrivial band structure in Sb_2Te_3: (a) calculated band structure along the $\bar{K}$-$\bar{\Gamma}$-$\bar{M}$ cut of the Sb_2Te_3(111) BZ. Bulk band projections are represented by the shaded areas. The bulk (surface) band structure results with SOC are presented in blue (red lines) and that without SOC in green (black lines). (b) Schematic of the single surface spin-Dirac cone in Sb_2Te_3 based on calculations. (c) Enlargement of low energy region [shaded box in (a)] near $\bar{\Gamma}$. (d) Second derivative image of the bulk valence bands along $\bar{\Gamma}$-$\bar{M}$ and (e) $\bar{\Gamma}$-$\bar{K}$ at $k_z = -0.77$ Γ-Z. Corresponding bulk band calculations are superimposed.

Having identified a new topological insulator Bi_2Te_3, we proceed to investigate whether similar topological effects can take place in a non-bismuth-based compound. Figure 4(a) shows the calculated electronic structure of Sb_2Te_3, which, like Bi_2Te_3, exhibits a bulk insulating band structure that is strongly influenced by SOC and a single Dirac cone on its (111) surface. By comparing our SOC calculations with the experimentally measured bulk valence bands, it is clear that there is good agreement along both the k_x [Fig. 4(d)] and k_y [Fig. 4(e)] directions, showing that the bulk electronic structure of Sb_2Te_3 is consistent with having topologically nontrivial bulk properties. However, due to a high level of intrinsic doping that is typical of these compounds, the Fermi energy of naturally grown Sb_2Te_3 lies in the bulk valence band continuum and thus does not cut through the surface states. Unlike $Bi_{2-x}Mn_xTe_3$, no time dependence of the bands is observed. Recently, we came across independent work [29] on a different $Bi_2(Sn)Te_3$ series that finds a single Dirac cone.

In conclusion, our first-principles theoretical calculations and ARPES results show that Bi_2Te_3 and Sb_2Te_3 possess *bulk* band structures where the insulating gap originates from a large spin-orbit coupling term, and such insulators support topologically nontrivial Z_2 surface states. Our direct observation of single Dirac cones in these materials and the systematic methods demonstrated to control the Dirac fermion dynamics on these highly nontrivial surfaces point to new opportunities for spintronic and quantum-information materials research.

The use of synchrotron x rays and theoretical computations is supported by DOE/BES (No. DE-FG-02-05ER46200, No. AC03-76SF00098, and No. DE-FG02-07ER46352). Materials growth is supported by NSF (No. DMR-0819860). M. Z. H. acknowledges the A. P. Sloan Foundation.

*mzhasan@Princeton.edu

[1] C. Day, Phys. Today **62**, No. 4, 12 (2009).
[2] L. Fu, C. L. Kane, and E. J. Mele, Phys. Rev. Lett. **98**, 106803 (2007).
[3] J. E. Moore and L. Balents, Phys. Rev. B **75**, 121306(R) (2007).
[4] R. Roy, arXiv:cond-mat/0607531.
[5] D. Hsieh, D. Qian, L. Wray, Y. Xia, Y. Hor, R. J. Cava, and M. Z. Hasan, Nature (London) **452**, 970 (2008).
[6] D. Hsieh *et al.*, Science **323**, 919 (2009); Nature (London) **460**, 1101 (2009).
[7] Y. Xia *et al.*, Nature Phys. **5**, 398 (2009).
[8] Y. S. Hor *et al.*, Phys. Rev. B **79**, 195208 (2009).
[9] K. S. Novoselov *et al.*, Nature (London) **438**, 197 (2005).
[10] X.-L. Qi *et al.*, Phys. Rev. B **78**, 195424 (2008).
[11] A. P. Schnyder *et al.*, Phys. Rev. B **78**, 195125 (2008).
[12] A. Essin, J. E. Moore, and D. Vanderbilt, Phys. Rev. Lett. **102**, 146805 (2009).
[13] M. Franz, Physics **1**, 36 (2008).
[14] L. Fu and C. L. Kane, Phys. Rev. Lett. **102**, 216403 (2009).
[15] A. R. Akhmerov, J. Nilsson, and C. W. J. Beenakker, Phys. Rev. Lett. **102**, 216404 (2009).
[16] Y. Ran, Y. Zhang, and A. Vishwanath, Nature Phys. **5**, 298 (2009).
[17] B. Seradjeh, J. E. Moore, and M. Franz, Phys. Rev. Lett. **103**, 066402 (2009).
[18] B. Lenoir *et al.*, J. Phys. Chem. Solids **57**, 89 (1996).
[19] H. Zhang *et al.*, Nature Phys. **5**, 438 (2009).
[20] H.-J. Noh *et al.*, Europhys. Lett. **81**, 57 006 (2008).
[21] P. Blaha *et al.*, computer code WIEN2K, Vienna University of Technology, 2001.
[22] P. Perdew *et al.*, Phys. Rev. Lett. **77**, 3865 (1996).
[23] G. Wang and T. Cagin, Phys. Rev. B **76**, 075201 (2007).
[24] S. J. Youn and A. J. Freeman, Phys. Rev. B **63**, 085112 (2001).
[25] S. K. Mishra, S. Satpathy, and O. Jepsen, J. Phys. Condens. Matter **9**, 461 (1997).
[26] S. Urazhdin *et al.*, Phys. Rev. B **69**, 085313 (2004).
[27] G. A. Thomas *et al.*, Phys. Rev. B **46**, 1553 (1992).
[28] S. Hüfner, *Photoelectron Spectroscopy* (Springer, Berlin, 1995).
[29] Y. L. Chen *et al.*, arXiv:0904.1829v1.